A Prototype for Remote Monitoring of Ocean Heat Content

D. S. Trossman,[1] **R. H. Tyler**[2,3]

[1]Oden Institute for Computational Engineering and Sciences, University of Texas, Austin, TX, USA
[2]Geodesy and Geophysics Laboratory, Code 61A, NASA Goddard Space Flight Center, Greenbelt, MD, USA
[3]Joint Center for Earth Systems Technology, University of Maryland, Baltimore County, MD, USA

Key Points:

- Statistical model trained on hydrographic observations using satellite data could potentially monitor global ocean heat content (OHC)
- Root-mean-square error depends on variance of OHC in hydrographic transect observations and variables included in statistical model
- Changes in OHC could potentially be remotely monitored over sufficiently long time scales to sample enough training data

Corresponding author: David S. Trossman, trossman@oden.utexas.edu

Abstract

A new approach to monitor ocean heat content (OHC) is proposed to overcome challenges with observing OHC over the entire ocean. The output of an ocean state estimate (ECCO) is sampled along historical hydrographic transects, a machine learning algorithm (GAM) is trained on these samples, and OHC is estimated everywhere using information inferable from various global satellite coverage. Assuming the ECCO output is perfect observational data, a GAM can estimate OHC within 0.15% spatial root-mean-square error (RMSE). This RMSE is sensitive to the spatial variance in OHC that gets sampled by hydrographic transects, the variables included in the GAM, and their measurement errors when inferred from satellite data. OHC could be remotely monitored over sufficiently long time scales when enough spatial variance in OHC is explained in the training data over those time scales.

1 Introduction

In this paper, a prototype of a remote monitoring technique for ocean heat content is outlined. Since the 1970's, large-scale warming of the upper 700 m of the ocean has been observed (*Domingues et al.*, 2008; *Ishii and Kimoto*, 2009; *Durack and Wijffels*, 2010; *Levitus et al.*, 2012; *Abraham et al.*, 2013; *Balmaseda et al.*, 2013; *Lyman and Johnson*, 2014; *Roemmich et al.*, 2015; *Gleckler et al.*, 2016; *Boyer et al.*, 2016; *Ishii et al.*, 2017; *Cheng et al.*, 2017; *Zanna et al.*, 2019). Our ability to monitor the temperature of the upper 2000 meters in regions that aren't covered by sea ice has improved considerably since the 2000's, when Argo floats were first deployed (e.g., *Riser et al.*, 2016). However, below 2000 meters depth, we must rely on hydrography measured along ship tracks, which has been shown to provide insufficient sampling of the ocean's temperature at such deep depths (*Garry et al.*, 2019). Thus, the specific heat- and density-weighted depth-integral of temperature, which is referred to as "ocean heat content" (OHC), has been a challenge to accurately monitor. With the ocean taking up more than 93% of the excess heat accumulating on earth due to the presence of greenhouse gases humans have emitted (e.g., *Levitus et al.*, 2001; *Trenberth et al.*, 2014 and 2016; *von Schuckmann et al.*, 2016), the OHC has been considered a proxy for the Earth's energy imbalance and therefore a critical climate variable to monitor. Further, the associated ocean temperature increase has accounted for roughly half of the observed global mean sea level rise from 1972 to 2008 (*Church et al.*, 2011 and 2013; *Gregory et al.*, 2013) and about one-third of the observed global mean sea level rise since 2005 (*Chambers et al.*, 2017; *The WCRP sea level budget group*, 2018).

One widely accepted approach to monitoring OHC is to use multiple data assimilation-based modeling systems (e.g., *Trenberth et al.*, 2014 and 2016), but this substitutes the problem of incomplete observations with imperfect modeling systems. The approaches currently tend to use a combination of in situ observations of temperature (e.g., *Kouketsu et al.*, 2011; *Abraham et al.*, 2013; *Balmaseda et al.*, 2013; *Roemmich et al.*, 2015; *Gleckler et al.*, 2016; *Boyer et al.*, 2016; *Ishii et al.*, 2017; *Cheng et al.*, 2017; *Meyssignac et al.*, 2019) and fill in the spatial gaps with reanalysis data because ~13% of the OHC resides in regions, such as those covered by sea ice and at depths below 2000 meters (*Purkey and Johnson*, 2010), that are not well-sampled by observations (*Desbruyéres et al.*, 2016). However, there is considerable bias (*Garry et al.*, 2019) and uncertainty (*Llovel et al.*, 2014) in the extent of the unobserved OHC and warming of such regions has been increasing with time (*Gleckler et al.*, 2016). Furthermore, the spread in depth-integrated temperature anomalies in the upper 700 meters across ocean reanalyses is greater than the ensemble mean in many coastal and high latitude regions (*Palmer et al.*, 2017).

A number of independent approaches for monitoring OHC have been proposed. These include acoustic time travel measurements (*Munk and Wunsch*, 1979; *Dushaw et al.*, 2009), satellite altimetry observations of internal tides phase speed changes along their

ray paths (*Zhao*, 2016), atmospheric measurements of oxygen and carbon dioxide concentrations (Resplandy et al., 2019), theoretical and model-derived relationships between sea surface heights (from satellite altimetry) and bottom pressure (via satellite gravimetry) with ocean heat content (*Jayne et al.*, 2003; *Fasullo and Gent*, 2017), ocean net surface fluxes (radiative and turbulent adjusted for mass transfer) from space to get the net ocean heating rate (*L'Ecuyer et al.*, 2015), thermal expansion as a residual inferred from space-based observations and the sea level budget (*Chambers et al.*, 2017; *The WCRP sea level budget group*, 2018; *Hamlington et al.*, 2020), and depth-integrated electrical conductivity ("conductance") and depth-integrated conductivity-weighted velocity ("conductivity transport") measurements from in situ observations and inferred from satellite magnetometry (*Irrgang et al.*, 2017; *Irrgang et al.*, 2019). But no single method is known to be capable of monitoring changes in OHC accurately enough to resolve annual variations.

A combination of many of the above methods could be used in conjunction with a machine learning method to monitor OHC. Machine learning methods have a history rooted in statistical regression techniques (e.g., *Hastie et al.*, 2001). Their framework is useful for the purpose of calculating OHC because of established associations with sea surface height, bottom pressure, conductance, and seafloor depth (*Jayne et al.*, 2003; *Fasullo and Gent*, 2017; *Irrgang et al.*, 2019). One primary difference between a general linear regression technique and a machine learning method is that the latter needs to find a balance between the bias and variance of its predictions through a regularization term. This term prevents the machine learning method from overfitting to a particular training data set, so that the approach can be applied to other data sets for prediction purposes. In order to guarantee that the machine learning model does not overfit to the training data, a type of cross-validation method is typically applied by leaving out some of the training data, predicting those data, and repeating for different combinations of the training data set. Two examples of machine learning methods that are cast in a regression-like framework include the Generalized Additive Model (GAM; *Wood*, 2006; *Trossman et al.*, 2011) and the artificial neural network (e.g., *Hsieh and Tang*, 1998; *Wahl et al.*, 2015; *Lary et al.*, 2016; *Irrgang et al.*, 2019). In this study, we use a GAM to establish whether remotely monitoring OHC is possible using quantities that can be inferred using both in situ and satellite data: sea surface height, bottom pressure, conductance, seafloor depth, and conductivity transport.

The structure of this manuscript is as follows. First, we describe the GAM we use to calculate the OHC from several observables and outline the data that the GAM is trained on. We utilize model output from an ocean state estimate, the Estimating the Circulation & Climate of the Ocean (ECCO) framework, in order to examine whether conductivity transports are associated with OHC. We then assess the feasibility of our OHC monitoring strategy by evaluating the optimal combination of training data and variables included in the GAM. We accomplish this by minimizing the root-mean-square error (RMSE) between the model-derived OHC and the GAM-derived OHC. We begin to examine the sensitivity of the RMSE to errors in the observations in order to understand the consequences they have for our proposed OHC monitoring strategy. Finally, we examine the balance of using training data over relatively short time scales with the amount of data that grows over longer time scales in monitoring OHC changes.

2 Modeling system and observations

To accomplish our goal of establishing how accurate an observational network can monitor OHC before consideration of measurement uncertainty, we require a global realistic set of data that can be sampled for several variables. An ocean state estimate that is in excellent agreement with historical observations and their changes relative to ocean reanalyses [*Heimbach et al.*, 2019] is utilized here. We use version 4, revision 3 of the Estimating the Circulation & Climate of the Ocean (ECCOv4r3; *Fukumori et al.*, 2017) framework for the ocean state estimate, which is based on the Massachusetts Institute of

Technology general circulation model (MITgcm) from 1992 to 2015. The fields used for this analysis were generated by a re-run of ECCOv4r3 using the MITgcm, which we describe in the Supplementary Information along with more details of the ECCO framework. The model's output is sampled along historical hydrographic transects in order to train our statistical model and then the model's globally complete output is compared to the resulting statistical model's estimates of OHC.

2.1 Observed hydrographic transects

The hydrographic transects used in this study are taken from the World Ocean Circulation Experiment (WOCE) and the Climate Variability and Predictability (CLIVAR) programs. Specifically, we use transects that have adequate information about both temperature and salinity to calculate a stratification, density, and/or electrical conductivity (σ), as in previous studies that require one or more of these three quantities (e.g., *Kunze*, 2017). Because we will never measure OHC at every point in the ocean, it is not very practical to use observations at every point in the ocean to train the GAM and then estimate OHC at each location. Instead, we train the GAM along particular transects that have been sampled by ships and apply the GAM.

Along these transects, we sample the following variables from the ECCO output. Conductance (Σ) is strongly spatially correlated with OHC over much of the ocean (Fig. S1d). From the ship, the sea surface height (SSH) can be measured. The SSH anomaly is related to the sea level anomaly, which is primarily a function of OHC (Fig. S1b) and added mass. The deepest measurement taken from the ship can be used to infer the bottom pressure (p_b). Bottom pressure is important to account for the added mass contributions to sea level as a correction to using SSH as a proxy for OHC (Fig. S1c; *Jayne et al.*, 2003). Seafloor cables (e.g., *Schnepf et al.*, 2020), such as the Florida Cable, measure voltage differences, which are converted to an estimate of the conductivity-weighted depth-averaged flow velocity crossing the cable (*Sanford*, 1971) or what we refer to here as the cross-cable component of the conductivity transport vector $\mathbf{T}_\sigma$. Mooring arrays (e.g., *Lozier et al.*, 2019), such as OSNAP, provide both conductivities and velocities such that $\mathbf{T}_\sigma$ can be calculated as well. The conductivity transport's magnitude, $|\mathbf{T}_\sigma|$ is marginally well-correlated with OHC (Fig. S1f) and will be included as a predictor for OHC in the following analysis. However, because $\mathbf{T}_\sigma$ is not necessarily measured–in situ–along the same hydrographic transects as the other variables, there may be logistical difficulties with using all of these data to train a GAM that calculates OHC. This is why we examine the importance of including $\mathbf{T}_\sigma$ in the GAM in the present study. Lastly, the seafloor depth (H) can be inferred from ship-based measurements. H is important to account for because a deeper ocean has the capability to hold more heat at a given location (Fig. S1a). A GAM can update the relationship between OHC and a static field such as H when all other (above-listed) predictors are included over a relevant time scale; this is why the GAM needs updated training data for each time period over which the OHC is monitored.

SSH anomalies are routinely monitored by satellite altimetry over the global ocean, whereas p_b, Σ, and $\mathbf{T}_\sigma$ can potentially be inferred from satellite data. In particular, p_b can be inferred from satellite gravimetry [*Ponte et al.*, 2007]. Σ and $\mathbf{T}_\sigma$ may be inferred or constrained using electric and magnetic field observations (including observations by satellite magnetometers) and this paper therefore considers their use in a GAM. H has been inferred from ship-based and satellite measurements and is essentially time-invariant, requiring that the GAM be retrained at each time we want to estimate OHC. After being trained on transects of in situ measurements of SSH, p_b, Σ, H, and $\mathbf{T}_\sigma$, OHC can then be estimated using bathymetry and time-dependent satellite observations with a GAM of the form given in the Supplementary Information. Using the hypothetical measurement errors–also given in the Supplementary Information–we further examine what the practical limitations are to using SSH, p_b, Σ, H, $\mathbf{T}_\sigma$, or some subset of these variables, as predictors of OHC.

3 Results

We first find combinations of transects that have been historically observed by ship that can train the GAM to have a minimal spatial RMSE in estimating global OHC. By iterating the GAM training and estimation steps with single transects, all combinations of pairs of transects, all combinations of triplets of transects, and so on until all historical transects are included in the training step, we find several optimal combinations of transects that can be used to minimize the global RMSE in estimating OHC at each location with zero measurement errors for one example month (April of 1992). These combinations of transects can yield a spatial RMSE in estimating OHC of about 0.15-0.25% with all of the predictors listed in Eq. 3 of the Supplementary Information. The example combination of transects shown in Fig. 1 is an example of one that leads to minimal RMSE. This example includes most historical transect data in the Indian Ocean, several select hydrographic transects in the Atlantic Ocean (including the long-running AR07/OSNAP-West line), and nothing in the Pacific Ocean. Table 1 tabulates the RMSE using this example combination of transects, but with different combinations of predictors in Eq. 3 of the Supplementary Information. Table 1 demonstrates that a predictor that has a smaller correlation with OHC reduces the RMSE by less than a predictor that has a higher correlation with OHC when added to the GAM.

The most important factors that determine the spatial RMSE are the variables included in the GAM (Table 1) and the variance in OHC used to train the GAM. The minimization of spatial RMSE using a GAM often requires training data that sufficiently span the range and domain of the statistical model (e.g., *Trossman et al.*, 2011). The example shown in Fig. 1 satisfies that criterion, as there is an inverse relationship between the percent spatial RMSE of the GAM and the standard deviation of the OHC in the training (hydrographic transect) data per number of transects, regardless of whether errors in the satellite data are accounted for. This inverse relationship still holds when $\mathbf{T}_\sigma$ and other variables are excluded from the GAM (not shown), and with similar spatial RMSEs in estimated OHC (Table 1).

Next, we evaluate how the spatial RMSE for OHC estimates using Eq. 3 of the Supplementary Information can be impacted by the presence of measurement errors in the satellite data. The percent change in spatial RMSE due to a change in the ratio of the standard deviation of the added random noise to the mean value of the variable (i.e., percent change in spatial RMSE times the signal-to-noise ratio) is quantified in Fig. 2. Accounting for only one variable's measurement error, the sensitivity of the spatial RMSE to the level of noise is shown in Fig. 2a. This figure suggests that the spatial RMSE in OHC is most sensitive to conductance measurement errors when the other measurement errors are negligible and similarly sensitive to seafloor depth measurement errors when all other measurement errors are ignored. Accounting for all measurement errors simultaneously, the spatial RMSE in OHC is most sensitive to seafloor depth measurement errors (Fig. 2b). This is because the strongest correlation between OHC and any variable is between OHC and seafloor depth (Fig. S1a). However, because not all of the standard deviation levels we chose for measurement error magnitudes are well-known, we further examine how the sensitivity of spatial RMSE to measurement errors in the partial models included in Table 1. The spatial RMSE in OHC is most sensitive to bottom pressure–and similarly sensitive to conductance–in each of the partial models that excludes seafloor depth (Fig. 2c). When seafloor depth is included, the measurement errors associated with seafloor depth dominate the sensitivity in spatial RMSE to measurement errors. The measurement errors in each of the variables used in the GAM will be important to quantify if our technique is going to be practically applied to monitor OHC, but the variable that needs to be most accurately known is the one that changes the least and could be most well-observed: the seafloor depths.

Training the GAM using the transects shown in Fig. 1 and applying the GAM with measurement errors in the predictors to estimate OHC as above–but for each month as a

function of time–we can accurately estimate OHC relative to the ECCO output. Here, we exclude $\mathbf{T}_\sigma$ due to potential challenges with observing the velocities along hydrographic transects concurrently with the other variables and its relatively small impact on RMSE. Figure 3a shows the temporally averaged residuals of the GAM estimates at each location of the ocean over 1992-2015. The GAM-based OHC estimates are too small for each month over 1992-2015 primarily because he Arctic Ocean has not been sampled in the training data and because the global relationships between each of the predictors and OHC are different in the Arctic compared to the rest of the world. These temporal residuals are fairly constant over time in the shelf regions, but vary dramatically over time in the Arctic Ocean, as indicated by the temporal standard deviations of the residuals (Fig. 3b). The temporal RMSE becomes strongly correlated (0.9998) with the seafloor depth over long (> 10 year) time periods (Fig. 3c), suggesting that OHC could be remotely monitored over decadal timescales with a predictable RMSE. However, the biases in the global OHC estimates with the GAM are not highly predictable for each month, as evidenced by how the temporal standard deviation of the residuals (Fig. 3b) dominate the bias contribution to the temporal RMSE (Fig. 3c) and by the fair correlation between the GAM-based global OHC estimates and the ECCO-based global OHC estimates (0.5). Only coastal regions have statistically significant differences between the GAM-based estimates and the ECCO-based estimates of OHC (magenta crosses in Fig. 3c) and these regions have the smallest OHC.

The is an optimal balance between the amount of data used to train the GAM and the time periods for which the GAM is applied. Figs. 3d-f demonstrate that using hydrographic transects only for the year over which the GAM-based estimates are being applied does not necessarily reduce the temporal residuals, standard deviation of the residuals, or RMSE. The residuals are largest in the same locations, whether all of the transects shown in Fig. 1 are used or only the transects for the year over which the GAM-based estimates are being applied (1-10 transects per year) are used. However, the (relatively small) differences between the residuals between use of these two training data sets are incoherent in their spatial patterns (Fig. 3d). The standard deviations of the residuals and the temporal RMSE also look similar, regardless of which training data set is used, but both the standard deviations of the residuals (Fig. 3e) and the temporal RMSE (Fig. 3f) are larger in open ocean regions when the transects for the year over which the GAM-based estimates are being applied are used. This is an example of how the number of transects used to train the GAM can be more important for accuracy of GAM-based estimates than use of the relevant times to train the GAM, but the opposite can also happen (e.g., if less transects were used than shown in Fig. 1).

4 Conclusions

Using the output of an ocean state estimate (ECCO), we trained a statistical model (GAM) on SSH, p_b, Σ, H, and $|\mathbf{T}_\sigma|$ across hydrographic transects, and demonstrated that this GAM can be used to accurately monitor global OHC to within about 0.15% RMSE on yearly time scales, assuming perfect information (i.e., no measurement errors and no sampling/aliasing/retrieval problems). When measurement errors are accounted for and global satellite observational coverage is attainable, measurement errors associated with seafloor depths were shown to dominate all others for the variable the machine learning algorithm is most sensitive to. The remote monitoring system proposed here can have a spatial RMSE that is $O(0.1\%)$ over monthly time scales, but our proposed remote OHC monitoring system only captures the temporal variability of global OHC with only fair temporal correlation, suggesting that it may not be possible to monitor OHC on such short time scales using our proposed remote sensing system. However, the temporal correlation is not high because of the limited variance in OHC captured by the training data for the GAM over such short time scales. This implies that our proposed remote monitoring system could distinguish OHC changes over sufficiently long time scales that enough training

data is collected. Further, if ocean warming accelerates, as it is expected to, the changes in OHC will be easier to detect over shorter time scales.

The RMSE for OHC estimates can further increase due to difficulties with constraining target variables from satellite data, incomplete sampling, and aliasing. In situ electromagnetic measurements (e.g., seafloor cables and eXpendable Current Profilers, XCPs) can be used to constrain Σ and $\mathbf{T}_\sigma$. XCPs estimate the horizontal vector $\mathbf{T}_\sigma$; cable voltage measurements give the component of $\mathbf{T}_\sigma$ crossing the cable and integrated along the cable; and remote magnetic data can provide the component of $\mathbf{T}_\sigma$ crossing contours of the ratio of the radial component of the magnetic field to Σ. However, these measurements are not as commonly performed as measurements for other variables (e.g., Conductivity, Temperature, and Depth, or CTD, which often discard σ data after salinity is calculated). Because a method to constrain Σ and $\mathbf{T}_\sigma$ by satellite magnetometry has not been well-established, we discussed the value of Σ and $\mathbf{T}_\sigma$ for estimating OHC separately. Further, some satellite data have experienced time periods with less-than-global coverage. For example, throughout much of the 1990's, SSH was observed using satellite altimetry between 66^oS and 66^oN and not in polar regions. Only including SSH at these locations increases RMSE of OHC estimate by less than 0.1%. Another factor that can impact the RMSE for OHC estimates is the sampling frequency and coverage from hydrography for the training step of the GAM. These factors will need to be accounted for if our proposed technique is going to be used to monitor OHC.

Some future research directions could refine our proposed remote monitoring system. First, measurement errors for each of the variables included in the GAM need to be refined. Second, additional training observations could improve the accuracy of the OHC estimates. Deep Argo and Arctic hydrographic transects could make a valuable additions to the hydrographic training data used here, which can be explored in a follow-up implementation study. Supplementing hydrographic observations from deep Argo observations could increase the variance in OHC in the training data and therefore reduce the RMSE of the OHC estimates. Finally, the opportunity for extracting Σ and $\mathbf{T}_\sigma$ is currently being explored by several research groups. A future study will ultimately make use of all available observations from at least as far back in time as 2002 to derive a time series and map of OHC with uncertainties and compare with other existing methods to estimate OHC. Furthermore, future investigations could inspect the potential to monitor freshwater fluxes into the ocean, heat transport, and/or tsunamis (e.g. *Manoj et al.*, 2010) using a similar approach to the one used in the present study.

Acknowledgments

David Trossman was supported by the NASA SLCT grant 80NSSC17K0558 and NASA PO pilot grant 80NSSC19K1664 at the University of Texas-Austin. The author acknowledges the Texas Advanced Computing Center (TACC) at The University of Texas at Austin for providing HPC resources for the ECCO simulations. The model data used in this study will be available at:

`https://zenodo.org/deposit/3897466`

upon publication, but for now are available at:

`https://utexas.box.com/s/b9ark937l90v00b96drrcemaen0zck3n`

References

Abraham, J. P., et al. (2013), A review of global ocean temperature observations: Implications for ocean heat content estimates and climate change, Rev. Geophys., 51, 450–483, doi:10.1002/rog.20022.

Balmaseda, M. A., K. E. Trenberth, E. Källén (2013), Distinctive climate signals in reanalysis of global ocean heat content, Geophys. Res. Lett., 40, 1754–1759, doi:10.1002/grl.50382.

Boyer, T., et al. (2016), Sensitivity of global upper-ocean heat content estimates to mapping methods, XBT bias corrections, and baseline climatologies, *J. Clim.*, **29**, 4817–4842.

Chambers, D. P., A. Cazenave, N. Champollion, H. Dieng, W. Llovel, R. Forsberg, R. (2017), Evaluation of the global mean sea level budget between 1993 and 2014, *Surv. Geophys.*, **38**:309. doi: 10.1007/s10712-016-9381-3

Chen, X., X. Zhang, J. A. Church, C. S. Watson, M. A. King, D. Monselesan, B. Legresy, C. Harig (2017), The increasing rate of global mean sea-level rise during 1993-2014, *Nature Clim. Change*, **7**, 492–495, doi:10.1038/nclimate3325.

Cheng, L. et al. (2016), XBT science: assessment of instrumental biases and errors, *Bull. Am. Meteorol. Soc.*, **97**, 924–933.

Cheng, L., K. E. Trenberth, J. Fasullo, T. Boyer, J. Abraham, J. Zhu (2017), Improved estimates of ocean heat content from 1960 to 2015, *Science Adv.*, **3**:e1601545.

Church, J. A., N. J. White, L. F. Konikow, C. M. Domingues, J. G. Cogley, E. Rignot, J. M. Gregory, M. R. van den Broeke, A. J. Monaghan, I. Velicogna (2011), Revisiting the Earth's sea-level and energy budgets from 1961 to 2008, *Geophys. Res. Lett.*, **38**, L18601, doi:10.1029/2011GL048794.

Church, J. A., Clark, P. U., Cazenave, A., Gregory, J. M., Jevrejeva, S., Levermann, A., Merrifield, M. A., Milne, G. A., Nerem, R. S., Nunn, P. D., Payne, A. J., Pfeffer, W. T., Stammer, D., Unnikrishnan, A. S.: Sea level change, in: Climate Change (2013), The Physical Science Basis, edited by: Stocker, T. F., Qin, D., Plattner, G.-K., Tignor, M., Allen, S. K., Boschung, J., Nauels, A., Xia, Y., Bex, V., Midgley, P. M., Contribution of Working Group I to the Fifth Assessment Report of the Intergovernmental Panel on Climate Change (Cambridge University Press, Cambridge, United Kingdom and New York, NY, USA), 2013.

Desbruyéres, D. G., S. G. Purkey, E. L. McDonagh, G. C. Johnson, B. A. King (2016), Deep and abyssal ocean warming from 35 years of repeat hydrography, *Geophys. Res. Lett.*, **43**, 10,356–10,365, doi:10.1002/2016GL070413.

Domingues, C. M., J. A. Church, N. J. White, P. J. Gleckler, S. E. Wijffels, P. M. Barker, J. R. Dunn (2008), Improved estimates of upper-ocean warming and multi-decadal sea level rise, *Nature Lett.*, **453**(19), doi:10.1038/nature07080.

Durack, P. J., S. E. Wijffels (2010), Fifty-year trends in global ocean salinities and their relationship to broad-scale warming, *J. Clim.*, **23**, 4342–4362.

Dushaw, B. D., et al. (2009), A decade of acoustic thermometry in the North Pacific Ocean, *J. Geophys. Res.*, **114**, C07021, doi:10.1029/2008JC005124.

Fasullo, J. T., P. R. Gent (2017), On the relationship between regional ocean heat content and sea surface height, *J. Clim.*, **30**, 9195–9211.

Frederikse, T., S. Jevrejeva, R. E. M. Riva, S. Dangendorf (2018), A consistent sea-level reconstruction and its budget on basin and global scales over 1958-2014, *J. Clim.*, **31**, 1267–1280.

Fukumori, I., O. Wang, I. Fenty, G. Forget, P. Heimbach, R. M. Ponte (2017), ECCO Version 4 Release 3, DSpace@MIT, http://hdl.handle.net/1721.1/110380.

Garner, A. J., J. L. Weiss, A. Parris, R. E. Kopp, R. M. Horton, J. T., Overpeck, B. P. Horton (2018), Evolution of 21st century sea-level rise projections, *Earth's Future*, doi:10.1029/2018EF000991.

Garry, F. K., E. L. McDonagh, A. T. Blaker, C. D. Roberts, D. G. Desbruyéres, E. Frajka-Williams, B. A. King (2019), Model-derived uncertainties in deep ocean temperature trends between 1990 and 2010, *J. Geophys. Res.-Oceans*, **124**, 1155–1169. https://doi.org/10.1029/2018JC014225

Gleckler, P. J., P. J. Durack, R. J. Stouffer, G. C. Johnson, C. E. Forest (2016), Industrial-era global ocean heat uptake doubles in recent decades, *Nature Clim. Change*, **6**, 394–398, doi:10.1038/nclimate2915.

Gregory, J. M., N. J. White, J. A. Church, M. F. P. Bierkens, J. E. Box, M. R. Van den Broeke, J. G. Cogley, X. Fettweis, E. Hanna, P. Huybrechts, L. F. Konikow, P. W. Leclercq, B. Marzeion, J. Oerlemans, M. E. Tamisiea, Y. Wada, L. M. Wake, R. S. W. Van de Wal (2013), Twentieth-century global-mean sea level rise: is the whole greater than the sum of the parts? *J. Clim.*, **26**, 4476–4499.

Griffies, S. M., et al. (2014), An assessment of global and regional sea level for years 1993-2007 in a suite of inter annual CORE-II simulations, *Ocean Modelling*, **78**, 35-89, doi:10.1016/j.ocemod.2014.03.004.

Hamlington, B. D., A. Burgos, P. R. Thompson, F. W. Landerer, C. G. Piecuch, S. Adhikari, L. Caron, J. T. Reager, E. R. Ivins (2018), Observation-driven estimation of the spatial variability of 20th century sea level rise, *J. Geophys. Res.-Oceans*, **123**, 2129–2140, doi:10.1002/2017JC013486.

Hamlington, B. D., A. S. Gardner, E. Ivins, J. T. M. Lenaerts, J. T. Reager, D. S. Trossman, E. D. Zaron, S. Adhikari, A. Arendt, A. Aschwanden, B. D. Beckley, D. P. S. Bekaert, G. Blewitt, L. Caron, H. A. Chandanpurkar, K. Christianson, R. I. Cullather, R. M. DeConto, J. T. Fasullo, T. Frederikse, J. T. Freymueller, D. M. Gilford, M. Girotto, W. C. Hammond, R. Hock, N. Holschuh, R. E. Kopp, F. Landerer, E. Larour, D. Menemenlis, M. Merrifield, J. X. Mitrovica, R. S. Nerem, I. J. Nias, V. Nieves, S. Nowicki, K. Pangaluru, C. G. Piecuch, D. R. Rounce, N.-J. Schlegel, H. Seroussi, M. Shirzaei, I. Velicogna, N. Vinogradova, T. Wahl, D. N. Wiese, M. J. Willis (2020), Understanding of contemporary regional sea-level change and the implications for the future. *Reviews of Geophysics*, **58**, e2019RG000672. https://doi.org/10.1029/2019RG000672

Hastie, T., R. Tibshirani,J. Friedman (2001), The Elements of Statistical Learning: Data Mining, Inference, and Prediction. Springer Verlag, 533 pp.

Heimbach, P., I. Fukumori, C. N. Hill, R. M. Ponte, D. Stammer, C. Wunsch, J.-M. Campin, B. Cornuelle, I. Fenty, G. Forget, A. K ohl, M. Mazloff, D. Menemenlis, A. T. Nguyen, C. Piecuch, D. Trossman, A. Verdy, O. Wang, H. Zhang (2019), Putting it all together: Adding value to the global ocean and climate observing systems with complete self-consistent ocean state and parameter estimates, *Frontiers in Marine Science*, **6**:55, doi:10.3389/fmars.2019.00055.

Hsieh, W. W., B. Tang (1998), Applying Neural Network Models to Prediction and Data Analysis in Meteorology and Oceanography, *B. Am. Meteorol. Soc.*, **79**(9), 1855–1870.

Irrgang, C., J. Saynisch, M. Thomas (2017). Utilizing oceanic electromagnetic induction to constrain an ocean general circulation model: A data assimilation twin experiment, *Journal of Advances in Modeling Earth Systems*, **9**, 1703–1720. https://doi.org/10.1002/2017MS000951

Irrgang, C., J. Saynisch, M. Thomas (2019), Estimating global ocean heat content from tidal magnetic satellite observations, *Nature Sci. Rep.*, **9**:7893, https://doi.org/10.1038/s41598-019-44397-8.

Ishii, M., M. Kimoto (2009), Reevaluation of historical ocean heat content variations with time-varying XBT and MBT depth bias corrections, *J. Oceanogr.*, **65**, 287–299.

Ishii, M. et al. (2017), Accuracy of global upper ocean heat content estimation expected from present observational data sets, *Sci. Online Lett. Atmos.*, **13**, 163–167.

Jayne, S. R., J. M. Wahr, F. O. Bryan, 2003: Observing ocean heat content using satellite gravity and altimetry. *J. Geophys. Res.*, **108**(C2), 3031, doi:10.1029/2002JC001619.

Johnson, G. C., J. M. Lyman, S G. Purkey (2015), Informing deep Argo array design using Argo and full-depth hydrographic section data, *J. Atmos. Ocean. Technol.*, **32**, 2187–

2198

Johnson, G. C., J. M. Lyman, N. G. Loeb (2016), Improving estimates of Earth's energy imbalance, *Nature Clim. Change Correspondence*, **6**.

Kalmikov, A. G., P. Heimbach (2014), A Hessian-based method for uncertainty quantification in global ocean state estimation, *SIAM Journal on Scientific Computing*, **36**, S267–S295.

Kalmikov, A. G., P. Heimbach (2018), On barotropic mechanisms of uncertainty propagation in estimation of Drake Passage transport, arXiv.org.

Kouketsu, S. et al. (2011), Deep ocean heat content changes estimated from observation and reanalysis product and their influence on sea level change, *J. Geophys. Res. Oceans*, **116**(3), 1–16.

Kunze, E. (2017), Internal-wave-driven mixing: Global geography and budgets, *J. Phys. Oceanogr.*, **47**, 1325–1345.

Lary, D. J., A. H. Alavi, A. H. Gandomi, A. L. Walker (2016), Machine learning in geosciences and remote sensing, *Geosci. Front.*, **7**(1), 3–10.

L'Ecuyer, T., H. K. Beaudoing, M. Rodell, W. Olson, B. Lin, S. Kato (2015), The observed state of the energy budget in the early 21st century, *J Clim*. **28**, 8319–8346. doi: 10.1175/JCLI-D-14-00556.1

Levitus, S., J. I. Antonov, J. Wang, T. L. Delworth, K. W. Dixon, A. J. Broccoli (2001), Anthropogenic warming of Earth's climate system, *Science*, **292**(5515), 267–270, doi:10.1126/science.1058154.

Levitus, S., et al. (2012), World ocean heat content and thermosteric sea level change (0-2000 m), 1955-2010, *Geophys. Res. Lett.*, **39**, L10603, doi:10.1029/2012GL051106.

Loeb, N. G., et al. (2012), Observed changes in top-of-the-atmosphere radiation and upper-ocean heating consistent within uncertainty, Nature Geosci. 5, 110–113

Lozier, M. S., F. Li, S. Bacon, F. Bahr, A. S. Bower, S. A. Cunningham, M. F. de Jong, L. de Steur, B. deYoung, J. Fischer, S. F. Gary, B. J. W. Greenan, N. P. Holliday, A. Houk, L. Houpert, M. E. Inall, W. E. Johns, H. L. Johnson, C. Johnson, J. Karstensen, G. Koman, I. A. Le Bras, X. Lin, N. Mackay, D. P. Marshall, H. Mercier, M. Oltmanns, R. S. Pickart, A. L. Ramsey, D. Rayner, F. Straneo, V. Thierry, D. J. Torres, R. G. Williams, C. Wilson, J. Yang, I. Yashayaev, J. Zhao (2019), A sea change in our view of overturning in the subpolar North Atlantic, *Science*, **363**, 516–521.

Lyman, J. M., G. C. Johnson (2008), Estimating annual global upper-ocean heat content anomalies despite irregular in situ ocean sampling, *J. Clim.*, **21**, 5629–5641.

Lyman, J. M., et al. (2010), Robust warming of the global upper ocean, *Nature*, **465**, 334–337

Lyman, J. M., G. C. Johnson, (2014), Estimating global ocean heat content changes in the upper 1800 m since 1950 and the influence of climatology choice, *J. Clim.*, **27**, 1945–1957

Manoj, C., A. Kuvshinov, S. Neetu, T. Harinarayana (2010), Can undersea voltage measurements detect tsunamis? *Earth, Planets and Space*, **62**, 353–358.

Meyssignac, B, T. Boyer, Z. Zhao, M. Z. Hakuba, F. W. Landerer, D. Stammer, A. Köhl, S. Kato, T. L'Ecuyer, M. Ablain, J. P. Abraham, A. Blazquez, A. Cazenave, J. A. Church, R. Cowley, L. J. Cheng, C. M. Domingues, D. Giglio, V. Gouretski, M. Ishii, G. C. Johnson, R. E. Killick, D. Legler, W. Llovel, J. Lyman, M. D. Palmer, S. Piotrowicz, S. G. Purkey, D. Roemmich, R. Roca, A. Savita, K. von Schuckmann, S. Speich, G. Stephens, G. J. Wang, S. E. Wijffels, N. Zilberman (2019), Measuring global ocean heat content to estimate the earth energy imbalance, *Frontiers in Marine Science*. **6**, doi:10.3389/fmars.2019.00432.

Munk, W., C. Wunsch (1979), Ocean acoustic tomography: a scheme for large scale monitoring, *Deep-Sea Res.*, **26**A, 123–161.

Nerem, R. S., D. P. Chambers, C. Choe, G. T. Mitchum (2010), Estimating mean sea level change from the TOPEX and Jason Altimeter Missions, *Marine Geodesy*, **33**(S1), 435–446, doi:10.1080/01490419.2010.491031.

Nerem, R. S., B. D. Beckley, J. T. Fasullo, B. D. Hamlington, D. Masters, G. T. Mitchum (2018), Climate-change-driven accelerate sea-level rise detected in the altimeter era, *PNAS*, **115**(9), 2022-2025, doi:10.1073/pnas.1717312115.

Ocaña, V., E. Zorita, P. Heimbach (2016), Stochastic secular trends in sea level rise, *J. Geophys. Res.-Oceans*, **121**, 2183–2202, doi:10.1002/2015JC011301.

Palmer, M. D., et al. (2017), Ocean heat content variability and change in an ensemble of ocean reanalyses, *Clim. Dyn.*, **49**, 909–930, doi:10.1007/s00382-015-2801-0.

Palter, J. B., S. M. Griffies, B. L. Samuels, E. D. Galbraith, A. Gnanadesikan, A. Klocker (2014), The deep ocean buoyancy budget and its temporal variability, *J. Clim.*, **27**, 551–573.

Palter, J. B., C.-A. Caron, K. L. Law, J. K. Willis, D. S. Trossman, I. M. Yashayaev, D. Gilbert (2016), Variability of the directly-observed, mid-depth subpolar North Atlantic circulation, *Geophys. Res. Lett.*, **42**, doi:10.1002/2015GL067235.

Petereit, J., J. Saynisch-Wagner, C. Irrgang, M. Thomas, 2019: Analysis of ocean tide-induced magnetic fields derived from oceanic in situ observations: Climate trends and the remarkable sensitivity of shelf regions. *Journal of Geophysical Research-Oceans*, **124**, 8257–8270. https://doi.org/10.1029/2018JC014768

Piecuch, C. G., R. M. Ponte (2011), Mechanisms of interannual steric sea level variability, *Geophys. Res. Lett.*, **38**, L15605, doi:10.1029/2011GL048440.

Piecuch, C. G., R. M. Ponte (2014), Mechanisms of global-mean steric sea level change, *J. Clim.*, **27**, 824–834.

Piecuch, C. G., R. M. Ponte, C. M. Little, M. W. Buckley, I. Fukumori (2017), Mechanisms underlying recent decadal changes in sub polar North Atlantic Ocean heat content, *J. Geophys. Res.-Oceans*, **122**, 7181–7197, doi:10.1002/2017JC012845.

Ponte, R. M., K. J. Quinn, C. Wunsch, P. Heimbach (2007), A comparison of model and GRACE estimates of the large-scale seasonal cycle in ocean bottom pressure, *Geophys. Res. Lett.*, **34**, L09603, doi:10.1029/2007GL029599.

Purkey, S. G., G. C. Johnson (2010), Warming of global abyssal and deep Southern Ocean between the 1990s and the 2000s: Contributions to global heat and sea level rise budgets, *J. Clim.*, **23**, 6336–6351

Resplandy, L., R. F. Keeling, Y. Eddebbar, M. Brooks, R. Wang, L. Bopp, M. C. Long, J. P. Dunne, W. Koeve, A. Oschlies (2019), Quantification of ocean heat uptake from changes in atmospheric O2 and CO2 composition. *Scientific Reports*, **9**, 1–10. doi: 10.1038/s41598-019-56490-z

Rhein, M. et al. in Climate Change (2013), The Physical Science Basis (eds Stocker, T. F. et al.) 255–315 (IPCC, Cambridge University Press, 2013).

Riser, S. C., et al. (2016), Fifteen years of ocean observations with the global Argo array, *Nature Clim. Change*, **6**, 145–153, doi:10.1038/nclimate2872.

Roemmich, D., J. Church, J. Gilson, D. Monselesan, P. Sutton, S. Wijffels (2015), Unabated planetary warming and its ocean structure since 2006, *Nature Clim. Change*, **5**, 240–245, doi:10.1038/nclimate2513.

Sabaka, T. J., R. H. Tyler, N. Olsen, A. Kuvshinov, 2015: CM5, a pre-Swarm comprehensive geomagnetic field model derived from over 12yr of CHAMP, rsted, SAC-C and observatory data. *Geophysical Journal International*, **200**(3), 1596–1626. doi: 10.1093/gji/ggu493

Sabaka, T. J., R. H. Tyler, R. H., N. Olsen, 2016: Extracting ocean-generated tidal magnetic signals from Swarm data through satellite gradiometry. *Geophysical Research Letters*, **43**(7), 3237–3245.

Sabaka, T. J., L. Tøffner-Clausen, N. Olsen, C. C. Finlay, 2018: A comprehensive model of Earth's magnetic field determined from 4 years of Swarm satellite observations. *Earth, Planets and Space*, **70**(1), 130. doi: 10.1186/s40623-018-0896-3

Sanford, T. B., 1971: Motionally induced electric and magnetic fields in the sea. *Journal of Geophysical Research*, **76**, https://doi.org/10.1029/JC076i015p03476, http://www.agu.org/pubs/crossref/1971/JC076i015p03476.shtml.

Schnepf , N. R., M. C. Nair, J. Velímský, N. P. Thomas, 2020: Can seafloor voltage cables be used to study large-scale circulation? An investigation in the Pacific Ocean. *Ocean Sci. Disc.*, https://doi.org/10.5194/os-2019-129

Send, U., G. Krahmann, D. Mauuary, Y. Desaubies, F. Gaillard, T. Terre, J. Papadakis, M. Taroudakis, E. Skarsoulis, C. Millot (1997), Acoustic observations of heat content across the Mediterranean Sea, *Nature Lett.*, **385**, 615–617.

Sonnewald, M., C. Wunsch, P. Heimbach (2018), Linear predictability: A sea surface height case study, *J. Clim.*, **31**, 2599–2611.

Srokosz, M. A., H. L. Bryden, H. L. (2015), *Science* http://dx.doi.org/10.1126/ science.1255575

Talley, L. D., et al. (2016), Changes in ocean heat, carbon content, and ventilation: A review of the first decade of GO-SHIP global repeat hydrography, *Annu. Rev. Mar. Sci.*, **8**, 185–215.

Trenberth, K. E., J. T. Fasullo, M. A. Balmaseda (2014), Earth's energy imbalance, *J. Clim.*, **27**, 3129–3144.

Trenberth, K. E., J. T. Fasullo, K. von Schuckmann, L. Cheng (2016), Insights into Earth's energy imbalance from multiple sources, *J. Clim.*, **29**, 7495–7505.

Trossman, D. S., L. Thompson, S. L. Hautala (2011), Application of Thin-Plate Splines in Two-Dimensions to Oceanographic Tracer Data, *Journal of Atmospheric and Oceanic Technology*, **28**(11), 1522–1538.

Tyler, R. H., S. Maus, H. L uhr, 2003: Satellite observations of magnetic fields due to ocean tidal flow. *Science*, **299**(5604), 239–241.

Tyler, R. H., T. P. Boyer, T. Minami, M. M. Zweng, J. R. Reagan (2017), Electrical conductivity of the global ocean, *Earth, Planets and Space*, **69**:156, doi:10.1186/s40623-017-0739-7.

von Schuckmann, K., M. D. Palmer, K. E. Trenberth, A. Cazenave, D. Chambers, N. Champollion, J. Hansen, S. A. Josey, N. Loeb, P.-P. Mathieu, B. Meyssignac, M. Wild (2016), An imperative to monitor Earth's energy imbalance, *Nature Clim. Change*, **6**, 138–144; doi:10.1038/nclimate2876.

Wahle, K., J. Staneva, H. Guenther (2015), Data assimilation of ocean wind waves using Neural Networks. A case study for the German Bight, *Ocean Model.*, **96**, 117–125.

The WCRP Global sea level budget group (2018), Global sea-level budget 1993–present. *Earth Syst. Sci. Data*, **10**, 1551–1590. doi: 10.5194/essd-10-1551-2018

Wood, S. N. (2006), Generalized Additive Models: An Introduction with R. Chapman and Hall/CRC Press, 410 pp.

Xue, Y., M. A. Balmaseda, T. Boyer, B. Ferry, S. Good, I. Ishikawa, A. Kumar, M. Rienecker, A. J. Rosati, Y. Rin (2012), A Comparative analysis of upper-ocean heat content variability from an ensemble of operational ocean reanalyses, *J. Clim.*, **25**, 6905–6929.

Zanna, L., S. Khatiwala, J. Gregory, J. Ison, P. Heimbach (2019), Estimates and Attribution of Atlantic Ocean Heat Content and Sea Level Change, *Proc. Natl. Acad. Sci. USA*, **116**(4), 1126–1131, doi:10.1073/pnas.1808838115.

Zhao, Z. (2016), Internal tide oceanic tomography, *Geophys. Res. Lett.*, **43**, 9157–9164, doi:10.1002/2016GL070567.

573 **Table 1.** The globally area-averaged percent root-mean-square errors (RMSE) between the ECCO-derived
574 ocean heat content (OHC) and the Generalized Additive Model (GAM)-derived OHC for many different
575 GAMs. The percent RMSE in OHC is computed by calculating the root-mean-square error between the
576 ECCO-derived OHC and the GAM-derived OHC and dividing by the area-averaged ECCO-derived OHC
577 ($\approx 4.1 \times 10^{12}$ J m^{-2}). No measurement errors were accounted for in these calculations so perfect information
578 along each of the randomly chosen hydrographic transects and inferred from the satellites is assumed. This
579 example uses data to predict OHC during April of 1992. The smoother functions, $f_n(\cdot)$, are different in each
580 row and for different $n = 1, ..., 6$. The tensor product functions, $g(\cdot)$, are also different in each row.

terms included in GAM: OHC= f_0+...	percent RMSE in OHC
$f_1(\text{SSH})$	43.6%
$f_1(p_b)$	5.51%
$f_1(\Sigma)$	5.92%
$f_1(H)$	0.60%
$f_1(\lvert\mathbf{T}_\sigma\rvert)$	41.4%
$f_1(\text{SSH}) + f_2(p_b)$	6.12%
$f_1(\text{SSH}) + f_2(p_b) + g(\text{SSH},p_b)$	6.10%
$f_1(\text{SSH}) + f_2(p_b) + f_3(\Sigma)$	1.92%
$f_1(\text{SSH}) + f_2(p_b) + f_3(\Sigma) + g(\text{SSH},p_b,\Sigma)$	0.93%
$f_1(\text{SSH}) + f_2(p_b) + f_3(\Sigma) + f_4(H)$	0.21%
$f_1(\text{SSH}) + f_2(p_b) + f_3(\Sigma) + f_4(H) + g(\text{SSH},p_b,\Sigma,H)$	0.15%
$f_1(\text{SSH}) + f_2(p_b) + f_3(\Sigma) + f_4(H) + f_5(\lvert\mathbf{T}_\sigma\rvert)$	0.21%
$f_1(\text{SSH}) + f_2(p_b) + f_3(\Sigma) + f_4(H) + f_5(\lvert\mathbf{T}_\sigma\rvert) + g(\text{SSH},p_b,\Sigma,H,\lvert\mathbf{T}_\sigma\rvert)$	0.15%

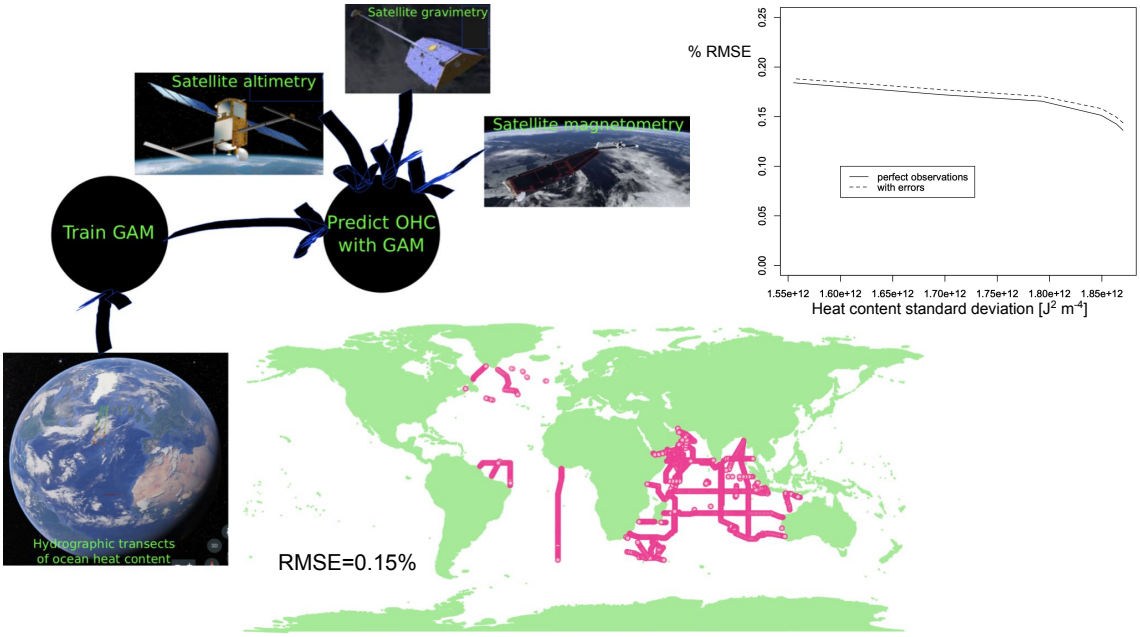

Figure 1. Flowchart for how the remote monitoring system for OHC would work. First, a Generalized Additive Model (GAM) is trained using hydrographic transect observations of ocean heat content, sea surface heights, bottom pressure, depth-integrated conductivity (conductance), and seafloor depth at hydrographic transect locations. Then the GAM is used at every wet point of the World Ocean where satellite altimetry (sea surface heights), gravimetry (bottom pressure), and magnetometry (conductance and conductivity transport) observations exist to estimate the OHC. Example relationships between the standard deviation of OHC from all training hydrographic transects per transect and the root-mean-square error (RMSE) of the resulting GAM via Eq. 3 of the Supplementary Information with and without considering errors in the satellite observations is shown. An example combination of hydrographic transect locations that determines one of the smallest RMSEs in estimated OHC, as determined by random sampling of every combination of hydrographic transects, is also shown, which includes: A01W,A14,AR04,AR07E,I01E,I01W,I02E,I02W,I03,I04,I05E,I07N,I09N,IR01W,IR03,IR04,IR06,ISS1,ISS2

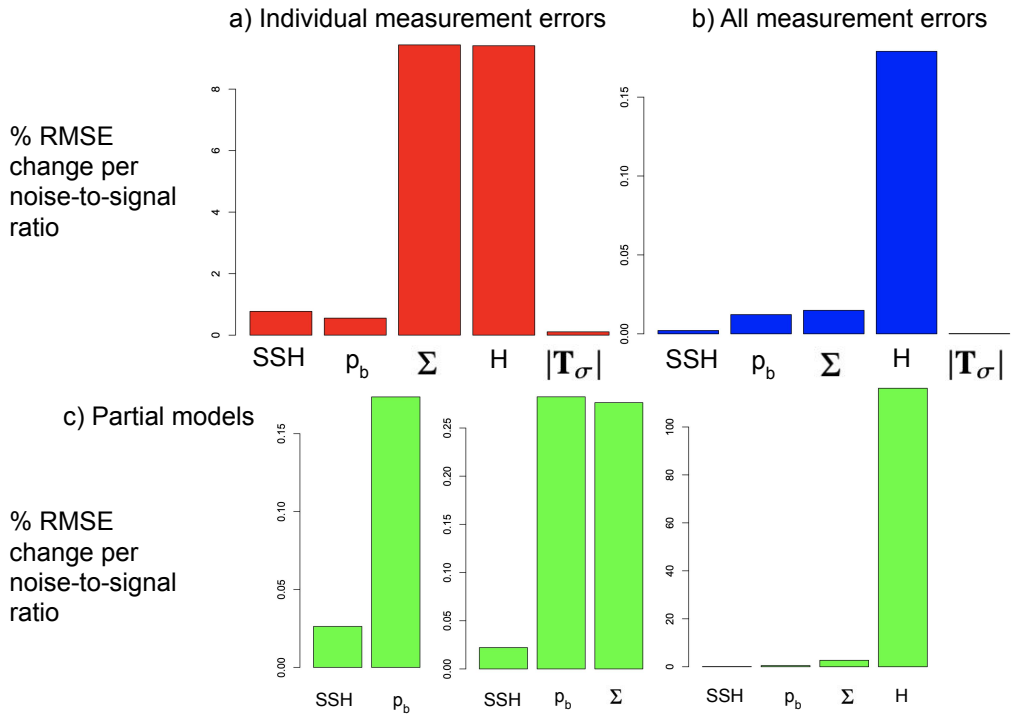

Figure 2. Some sensitivities of the RMSE from using Eq. 3 of the Supplementary Information due to measurement errors. Shown are: (a) the percent RMSE increase per noise-to-signal ratio due to measurement error for each individual variable's contribution (one at a time with no other errors), and (b) the same except accounting for all errors at once. (c) The bottom panels are the same as panel b, except for reduced models (those specified in Table 1): OHC$\sim$ $f_1(\text{SSH})+f_2(p_b)+g(\text{SSH},p_b)$, OHC$\sim$ $f_1(\text{SSH})+f_2(p_b)+f_3(\Sigma)+g(\text{SSH},p_b,\Sigma)$, OHC$\sim$ $f_1(\text{SSH})+f_2(p_b)+f_3(\Sigma)+f_4(H)+g(\text{SSH},p_b,\Sigma,H)$, and OHC$\sim$ $f_1(\text{SSH})+f_2(p_b)+f_3(\Sigma)+f_4(|\mathbf{T}_\sigma|)+g(\text{SSH},p_b,\Sigma,|\mathbf{T}_\sigma|)$ from left to right. The units of SSH are in meters, of p_b are in bars, of Σ are in S, of $|\mathbf{T}_\sigma|$ are in S m s^{-1}, and of H are in meters.

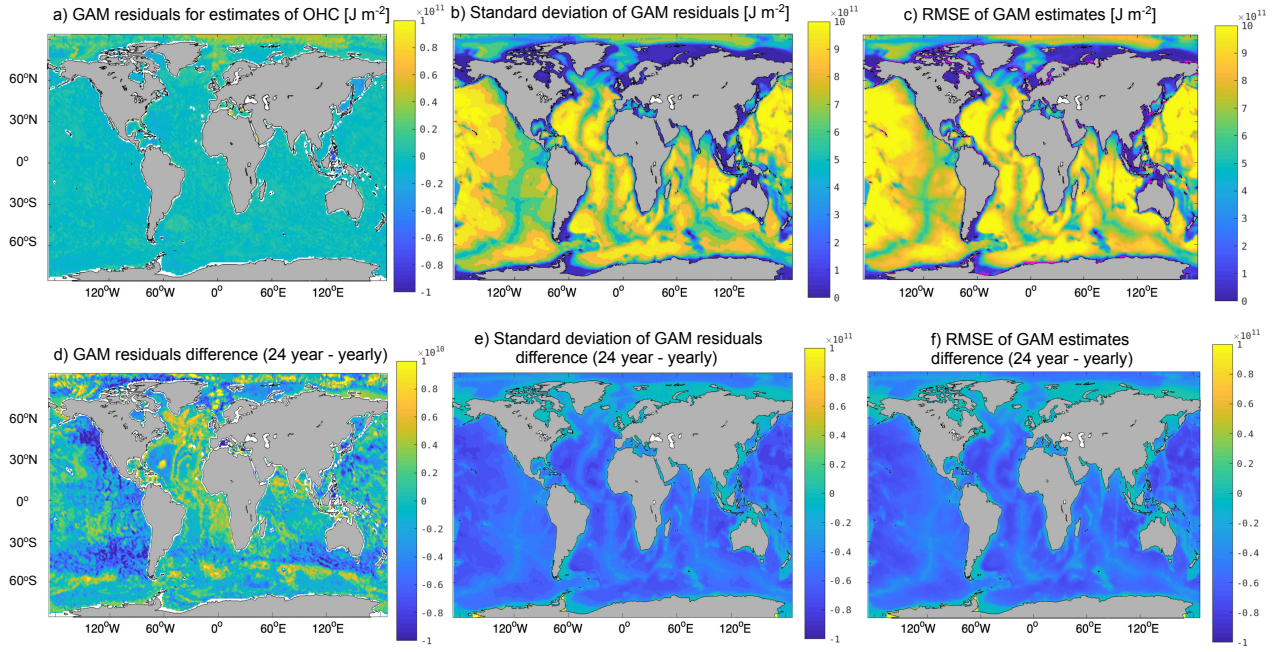

Figure 3. Including measurement errors in the data used to plug into the GAM and the transects shown in Fig. 1 for training data, shown are maps of (a) the temporally averaged residuals from the GAM-estimated OHC (units in J m^{-2}), (b) the temporal standard deviations of the residuals from the GAM-estimated OHC (units in J m^{-2}), and (c) the temporal root-mean-square errors (RMSEs) of the GAM-estimated OHC (units in J m^{-2}). Panel c includes magenta crosses wherever the GAM-estimated OHC is statistically significantly different from the ECCO-estimated OHC to the 95% confidence level, using 1.96 times the standard errors computed by the GAM as the half-width of the 95% confidence intervals. Also shown are the differences between the (d) temporally averaged residuals, (e) temporal standard deviations of the residuals, and (f) temporal RMSEs of the GAM-estimated OHC when trained on all transects shown in Fig. 1 and when trained only on transects from a given year for which the estimates are made ("yearly"). Yellow colors in panels d-f mean that values are greater using all transects shown in Fig. 1 and blue colors in panels d-f mean that values are greater using only transects from the given year for which the estimates are made.